

# Selection, Covariance, and Scaling Relations of Galaxy Clusters

B. Nord,<sup>1\*</sup> R. Stanek,<sup>2</sup> E. Rasia,<sup>1 4</sup> A.E. Evrard,<sup>1 2 3</sup>

<sup>1</sup>*Department of Physics, University of Michigan, 450 Church St., Ann Arbor, MI 48109-1040*

<sup>2</sup>*Department of Astronomy, University of Michigan, 500 Church St., Ann Arbor, MI 48109*

<sup>3</sup>*Michigan Center for Theoretical Physics, University of Michigan, 500 Church St., Ann Arbor, MI 48109*

<sup>4</sup>*Chandra Fellow*

Draft 1: March, 2007

## ABSTRACT

We explore how the behavior of galaxy cluster scaling relations are affected by flux-limited selection biases and intrinsic covariance among observable properties. Our models presume log-normal covariance between luminosity (L) and temperature (T) at fixed mass (M), centered on evolving, power-law mean relations as a function of host halo mass. Selection can mimic evolution; the L–M and L–T relations from shallow X-ray flux-limited samples will deviate from mass-limited expectations at nearly all scales while the relations from deep surveys ( $10^{-14}$  erg s $^{-1}$  cm $^{-2}$ ) become complete, and therefore unbiased, at masses above  $\sim 2 \times 10^{14} h^{-1} M_{\odot}$ . We derive expressions for low-order moments of the luminosity distribution at fixed temperature, and show that the slope and scatter of the L–T relation observed in flux-limited samples is sensitive to the assumed L–T correlation coefficient. In addition, L–T covariance affects the redshift behavior of halo counts and mean luminosity in a manner that is nearly degenerate with intrinsic population evolution.

**Key words:** clusters: general — clusters: ICM — clusters: cosmology — X-rays: clusters — clusters: calibration

## 1 INTRODUCTION

Encoded within observed galaxy cluster populations are important keys to cosmic structure evolution. The decryption of these clues requires an accurate understanding of survey selection. The character of the cluster population selected on an observable,  $\mathcal{O}$ , will depend strongly on how  $\mathcal{O}$  relates to the underlying halo mass and how that relation varies over time.

Upcoming surveys at sub-millimeter and optical wavelengths will complement existing efforts in the X-ray (Ebeling et al. 1998; Böhringer et al. 2002, 2006; Pierre et al. 2006) and optical (Miller et al. 2005; Koester et al. 2007) bands. Survey cross-calibration will enable detailed characterizations of the inter-relationships among observable tracers of mass. Precision cosmology derived from number counts and clustering (Levine et al. 2002; Majumdar & Mohr 2004; Lima & Hu 2004, 2005) relies on this type of interwoven tapestry.

Although efforts to understand cluster covariance will ultimately be pan-chromatic, this paper focuses on the behavior of two bulk X-ray properties—luminosity,  $L$ , and

temperature,  $T$ —derived from observations of flux-limited samples. In particular, we investigate how the form and evolution of the L–T relation depend on assumptions regarding the covariance in these observables with mass.

Dimensional arguments suggest power-law behaviors for the mean luminosity and temperature as a function of mass and epoch (Kaiser 1986). Recent work has moved beyond the slopes and intercept of this relation, focusing on a stochastic model with log-normal scatter about the mean population behavior (Reiprich & Böhringer 2002; Stanek et al. 2006; Reiprich 2006). The physical origin of this scatter has been linked to non-adiabatic mechanisms, such as cool cores (Fabian et al. 1996; Markevitch 1998; Arnaud & Evrard 1999; O’Hara et al. 2006) and mergers (Rowley et al. 2004; Poole et al. 2007). Analytic investigations discuss the impact of entropy floors on the scatter and evolution of the scaling relations among luminosity, temperature, and mass (Bower 1997; Balogh et al. 2006).

Self-similar evolution of the type envisaged by Kaiser (1986) has been tested with several observational samples, including those drawn from surveys from ASCA (Mushotzky & Scharf 1997; Novicki et al. 2002), XMM-Newton (Vikhlinin et al. 2002; Kotov & Vikhlinin 2005), CHANDRA (Lumb et al. 2004), and ROSAT (Fairley et al.

\* Email: bnord@umich.edu

2000; Maughan et al. 2006). These studies compare the L–T relation among redshift sub-populations in an effort to find the scaling with epoch. Results range from somewhat stronger than self-similar scaling to slightly negative. The work presented here addresses a potential source of confusion for such studies. Shallow flux-limited surveys are mass-incomplete, while samples derived from deeper flux-limited samples become complete at sufficiently high masses. This difference in selection, essentially a redshift-dependent Malmquist bias, manifests effects similar to genuine population evolution.

We work with two canonical flux limits,  $3 \times 10^{-12}$  and  $1 \times 10^{-14}$  ergs s $^{-1}$  cm $^{-2}$ , representative of the existing REFLEX survey and of future surveys such as ChaMP, XMM-LS and Spectrum X-Gamma<sup>1</sup>. We follow the conventions used in Stanek et al. (2006), where  $L$  is a rest-frame, soft-energy band (0.1 – 2.4 keV) X-ray luminosity in units of  $10^{44}$  ergs s $^{-1}$  with  $h = 0.7$  ( $H_0 = 100 h^{-1}$  km s $^{-1}$  Mpc $^{-1}$ ), and  $M$  is the mass within a sphere encompassing  $200\rho_c(z)$  in units of  $10^{15} h^{-1} M_\odot$ . Note the difference in Hubble constant conventions for luminosity and mass. We assume a concordance cosmology with a lower power spectrum normalization that is consistent with WMAP3 (Spergel et al. 2006):  $\{\Omega_m, \Omega_\Lambda, \sigma_8\} = \{0.3, 0.7, 0.8\}$ .

First, we discuss mass selection in the presence of scatter and flux limits and the consequences for X-ray cluster surveys (§2). We develop formalism in §3 for studies of correlated observable properties by introducing intrinsic covariance within a joint distribution of luminosity and temperature. Finally, we address the role of covariance in the study of scaling relation evolution.

## 2 L-M AND MASS SELECTION

We introduce the following notation for the logarithms of mass, luminosity, and temperature, respectively:  $\mu \equiv \ln M$ ,  $\ell \equiv \ln L$ , and  $t \equiv \ln T$ . We assume that the soft-band X-ray luminosity of halos follows a log-normal distribution with dispersion,  $\sigma_\ell$ , about a mean that varies with mass and epoch as

$$\bar{\ell} = \ell_{15,0} + p\mu + s \ln[E^2(z)]. \quad (1)$$

The normalization,  $\ell_{15,0}$ , defines the present-epoch geometric mean luminosity at the scale of  $10^{15} h^{-1} M_\odot$ ;  $p$  is the mass-scaling slope; and  $E(z) \equiv \sqrt{\Omega_m(1+z)^3 + \Omega_\Lambda}$  represents the Hubble parameter evolution for a flat metric. Our default model uses  $s = 1$ , appropriate for self-similar evolution in the soft X-ray band. The scatter  $\sigma_\ell$  is assumed to be mass- and redshift-independent. In what follows, we employ values  $p = 1.6$ ,  $\sigma_\ell = 0.59$ , and  $\ln L_{15,0} = 1.81$ , derived by matching REFLEX counts to predicted cluster counts to the Jenkins mass function (Stanek et al. 2006).

A sample’s flux threshold,  $f$ , sets a redshift-dependent luminosity limit,  $\ell_{min}(z) = \log[4\pi d_L^2(z) f/K(z, T)]$ , where the K-correction,  $K(z, T)$ , is detailed in the Appendix. Temperatures are discussed in §3.1 below. For non-negligible scatter,  $\sigma_\ell$ , this sharp luminosity-selection maps to a smooth selection, or window, function in mass

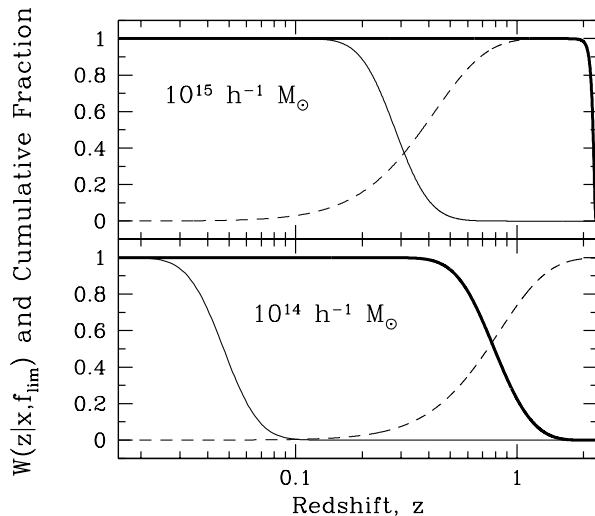


**Figure 1.** Window functions of current (solid) and next-generation (solid, bold) X-ray surveys are shown along with the cumulative fraction,  $N(< z)/N_{tot}$ , (dashed) of all halos at  $10^{15} h^{-1} M_\odot$  (upper) and  $10^{14} h^{-1} M_\odot$  (lower).

$$W(\mu, z) = \int_{\ell_{min}}^{\infty} d\ell \mathcal{P}(\ell|z, \mu) = \sqrt{\frac{\pi}{2}} \text{erfc}(\psi_{min}), \quad (2)$$

where  $\mathcal{P}(\ell|z, \mu)$  is a Gaussian distribution with mean given by equation (1) and constant scatter  $\sigma_\ell$ , and  $\psi_{min} \equiv [\ell_{min}(z, T) - \bar{\ell}(\mu, z)] / \sqrt{2}\sigma_\ell$ .

Fig. 1 displays the window functions of current and next-generation X-ray surveys for mass scales of the Coma-cluster ( $10^{15} h^{-1} M_\odot$ ) and for halos near the limits of modern Sunyaev-Zel’dovich surveys ( $10^{14} h^{-1} M_\odot$ , Holder & Carlstrom 2001). Dashed lines show the cosmic cumulative fraction,  $N(< z)/N_{tot}$ , of halos within redshift,  $z$ . For our chosen normalization  $\sigma_8 = 0.8$ , most  $10^{15} h^{-1} M_\odot$  halos lie within  $z = 1$ , while the  $10^{14} h^{-1} M_\odot$  population continues growing to  $z = 2$ . The next-generation window function allows detection of 100% of the  $10^{15} h^{-1} M_\odot$  halos in the sky. The decline in the window function at  $z \sim 0.5$  permits detection of  $\sim 56\%$  of the universal population at  $10^{14} h^{-1} M_\odot$ . By contrast, the shallow flux limits of current surveys detects only 34% and 0.06% of these totals.

Such incomplete mass sampling leads to a Malmquist bias that brightens the L–M relation relative to the intrinsic (mass-limited) population (Stanek et al. 2006). The log-mean luminosity of halos in a flux-limited sample is

$$\langle \ell(\mu) \rangle = \frac{\int dV(z) n(\mu, z) [\bar{\ell}(\mu, z) W(z|\mu) + \sigma_\ell e^{-\psi_{min}^2}]}{\int dN_f(\mu)}, \quad (3)$$

where  $dN_f(\mu) = dV(z) n(\mu, z) W(\mu, z)$ , represents the differential number of halos—within a comoving volume element,  $dV(z)$ —whose luminosities satisfy the threshold,  $\ell_{min}(z, T)$ . The second term manifests the bias such that when  $\psi_{min}$  becomes negligible and  $W$  remains appreciable (*i.e.*, when the median luminosity is near the flux limit), the geometric mean is enhanced by an amount comparable to the scatter,  $\sigma_\ell$ .

Fig. 2 compares the L–M relation for shallow and deep flux-limited surveys to the underlying, mass-limited relation. To discern between the effects of survey selection and

<sup>1</sup> <http://hea-www.harvard.edu/SXG/sxg.shtml>

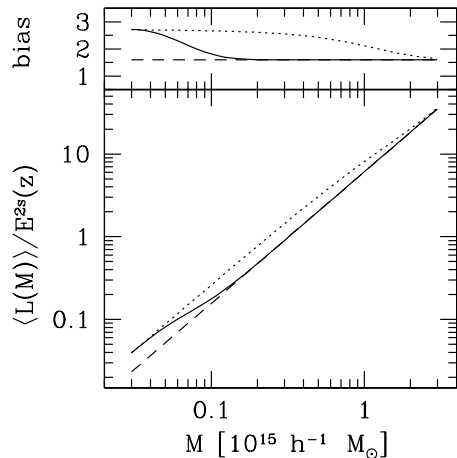


**Figure 2.** Geometric mean,  $\langle L \rangle \equiv e^{\langle \ell \rangle}$ , of the de-evolved luminosity for current (dotted) and next-generation (solid) flux-limited samples. The upper panel shows the bias relative to the underlying, mass-limited population (dashed).

redshift evolution, we plot the *de-evolved* geometric mean,  $\langle L/E^{2s} \rangle$ , using the model value,  $s = 1$ . Samples with the shallow flux limit show a gradual deviation from a power law at the high-mass end. At extremely high masses—above  $3 \times 10^{15} h^{-1} M_{\odot}$ —the bias disappears as the sample becomes mass-complete. For the deeper flux limit, surveys become mass-complete above  $2 \times 10^{14} h^{-1} M_{\odot}$  (see Fig. 1), and the resultant L–M relation is unbiased above this mass scale.

The deep sample probes to higher redshift than the shallow sample. But simply comparing the mean luminosity at fixed mass between these samples, without taking into account the evolving Malmquist bias, would produce an incorrect conclusion about luminosity evolution.

### 3 L–T AND CORRELATION

Since accurate total masses are difficult to obtain, existing studies have used X-ray temperature as a low-scatter mass proxy (Evrard et al. 1996). Several investigations of X-ray evolution have compared L–T relations among low- and high- redshift populations. Early work by Mushotzky & Scharf (1997), Fairley et al. (2000), and Novicki et al. (2002) find trends that are consistent with no evolution ( $s = 0$ ) to  $z \lesssim 0.8$ . A recent study by Maughan et al. (2006) compares the WARPS (Scharf et al. 1997) subsample with data from Arnaud & Evrard (1999) and Vikhlinin et al. (2002) to probe conventional and modified forms of self-similar evolution. They find consistency among the L–T slopes of differing redshift populations to be consistent with each other, but slightly *steeper* than the self-similar model. In a sample of 10 clusters at  $z > 0.4$ , Kotov & Vikhlinin (2005) measure evolution somewhat steeper than, but consistent with, self-similarity. Lumb et al. (2004) report near-self-similar evolution, and acknowledge the possibility of a flux-limit bias in their eight-cluster sample at  $0.45 < z < 0.62$ .

Balogh et al. (2006) compare observations with analytic models of the ICM, finding that the degree of evolution in the scaling relations depends strongly on that of the

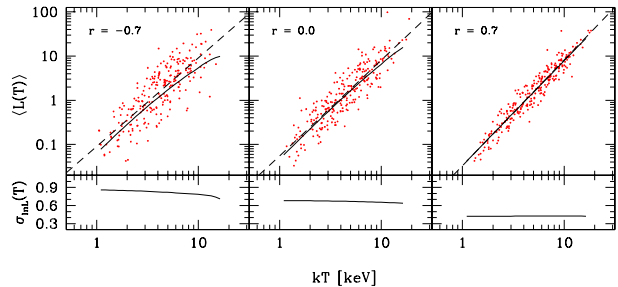


**Figure 3.** The X-ray luminosity–temperature relation (upper panels) and its dispersion  $\sigma_{\ell}(T)$  (lower panels) expected for current, flux-limited ( $3 \times 10^{-12} \text{ erg s}^{-1} \text{ cm}^{-2}$ ) samples and for different correlation coefficients,  $r = (-0.7, 0.0, 0.7)$ . Solid lines show the analytic expectations, points show discrete realizations from Hubble Volume full-sky halo realizations, and dashed lines are power-law fits to these discrete samples.

L–M scatter. Stanek et al. (2006) determine the redshift-independent  $\sigma_{\mu|\ell}$  in the presence of a flux-limit; they also note that simulations suggest a weak intrinsic correlation of the deviations in luminosity and temperature at fixed mass.

We next incorporate such covariance into scaling relation analysis. After computing observables under a multivariate Gaussian model, we add an explicit demonstration of the model using halos from Hubble Volume (HV) sky survey catalogues (Evrard et al. 2002). Our aim is to demonstrate the interplay between covariance and scaling relation parameters for flux-limited samples.

#### 3.1 Joint Luminosity-Temperature Distribution

To calculate the geometric mean and dispersion of the L–T relation, we assume that the log-mean temperature of the intracluster medium follows virial scaling behavior,

$$\bar{t} = t_{15} + \frac{2}{3}\mu + \frac{1}{3}\ln[E^2(z)], \quad (4)$$

with normalization  $t_{15} = \ln(kT_{15})$  and  $kT_{15} = 6.8 \text{ keV}$ . We further assume that there is constant log-normal scatter about the mean with  $\sigma_t = 0.10$ , equivalent to a 15% dispersion in mass at fixed temperature.

Using the normalized deviations,  $\delta_{\ell} \equiv (\ell - \bar{\ell})/\sigma_{\ell}$  and  $\delta_t \equiv (t - \bar{t})/\sigma_t$ , we form the joint log-normal distribution of luminosity and temperature at a given mass and epoch,

$$\mathcal{P}(\ell, t|\mu, z) = \frac{1}{2\pi R} e^{-\delta^T C^{-1} \delta}, \quad \delta \equiv \begin{bmatrix} \delta_{\ell} \\ \delta_t \end{bmatrix}, \quad (5)$$

where  $C_{ij} \equiv \langle \delta_i \delta_j \rangle$  is the correlation matrix with off-diagonal elements equal to the correlation coefficient,  $r \equiv \langle \delta_{\ell} \delta_t \rangle$ , and  $R \equiv \sqrt{1 - r^2}$ . The  $m^{\text{th}}$  moment of the distribution at fixed temperature is

$$\langle \ell^m(t) \rangle = \frac{\int dV(z) \int d\mu n(\mu, z) e^{-\delta_t^2/2} \mathcal{L}^{(m)}(t|\mu, z)}{\int dN_f(t)} \quad (6)$$

$$\mathcal{L}^{(m)}(t|\mu, z) = \int d\ell \ell^m \mathcal{P}(\ell|z, \mu, t), \quad (7)$$

where  $dN_f(t) = dV(z) d\mu n(\mu, z) W(\mu, z) e^{-\delta_t^2/2}$ . The first moment (*i.e.*, the geometric mean luminosity) is

$$\mathcal{L}^{(1)}(t|\mu, z) = W(\mu, z) \hat{\ell} + \sigma_{\ell} R e^{-\phi_{\text{min}}^2}, \quad (8)$$

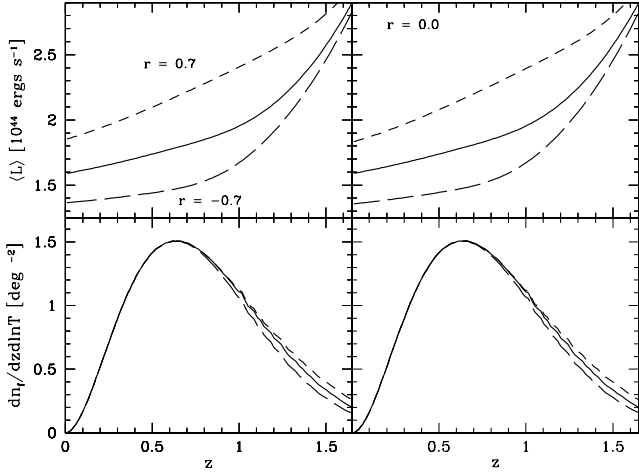


**Figure 4.** Redshift behavior of the geometric mean luminosity (upper) and the sky surface density (lower) of 4 keV clusters above a next-generation flux limit ( $10^{-14}$  erg s $^{-1}$  cm $^{-2}$ ). The solid line in all panels is our default model ( $s = 1$ ,  $\sigma_\ell = 0.59$ ,  $\ln L_{15,0} = 1.81$ ,  $r = 0$ ). The left panels vary the correlation coefficient,  $r = 0.7$  (short-dashed), and  $r = -0.7$  (long-dashed), otherwise retaining the default model parameters. The right panels hold  $r = 0$  and show the effects of changing the evolution and scatter:  $s = 0.95$ ,  $\sigma_\ell = 0.72$ ,  $\ln L_{15,0} = 1.65$  (long-dashed); and  $s = 1.1$ ,  $\sigma_\ell = 0.35$ ,  $\ln L_{15,0} = 1.95$  (short-dashed).

where  $\hat{\ell} \equiv \bar{\ell} + r \sigma_\ell \delta_t$  and  $\phi_{min} = (\ell - \hat{\ell}) / \sqrt{2} R \sigma_\ell$ . At a given mass, non-zero correlation effectively shifts the mean luminosity, either enhancing or suppressing the probability that a halo of given mass survives the flux cut. This has important implications in the counts and mean masses discussed below. In the no-correlation limit ( $r = 0$ ), equations (6) and (8) reduce to equation (3), but convolved with a temperature-selection filter.

From the L–T distribution’s second moment,

$$\mathcal{L}^{(2)}(t|\mu, z) = W(\mu, z) (\hat{\ell}^2 - R^2 \sigma_\ell^2) + e^{-\phi_{min}^2} (2R \sigma_\ell \hat{\ell} + \sqrt{2} R^2 \sigma_\ell^2 \phi_{min}), \quad (9)$$

we compute the observable variance,  $\sigma_\ell^2 = \langle \ell^2 \rangle - \langle \ell \rangle^2$ .

In Fig. 3, we show the expected L–T relation mean and dispersion for REFLEX flux-limited clusters assuming three degrees of L–T correlation,  $r \in (-0.7, 0.0, 0.7)$ . Points in the figure represent explicit realizations of the model derived from HV sky survey samples of massive halos above  $5 \times 10^{13} h^{-1} M_\odot$ . Using redshifts and masses of an all-sky survey, we assign luminosities and temperatures via equations (1) and (4), using two independent random Gaussian deviates,  $g_1$  and  $g_2$ :  $g_1$  controls the luminosity, and  $g_t = r g_1 + R g_2$  sets the temperature. We then apply a flux limit including K-correction terms.

Similar to the flux-limited L–M relation (Fig. 2), the L–T relation deviates from a pure power-law, although this deviation is extremely weak for values,  $r \gtrsim 0.5$ . The scatter depends strongly on the correlation coefficient, with magnitude varying from 0.8 to 0.4 as  $r$  varies from  $-0.7$  to  $0.7$ . Anti-correlation causes scatter orthogonal to the mean input relation, enhancing the magnitude of the observable dispersion. Positive correlation reduces this dispersion.

### 3.2 Evolution Diagnostics

For mass-complete samples, the mean L–T relation will behave as  $L \propto T^{3p/2} \rho_c(z)^{s-p/2}$ . For a flux-limited sample, the geometric mean soft-band luminosity at fixed temperature is

$$\langle \ell(z|t) \rangle = \frac{\int d\mu n(z, \mu) \int d\ell \ell \mathcal{P}(\ell|z, \mu, t)}{\int dn_f(z|t)}, \quad (10)$$

where  $dn_f(z|t) = d\mu n(\mu, z) W(\mu, z) e^{-\delta_t^2/2}$ . The luminosity in equation (10) and the sky surface density,  $(4\pi)^{-1} dV(z)/dz dn_f(z|t)$ , are shown in Fig. 4 for the case of  $kT = 4$  keV clusters selected with a next-generation ( $10^{-14}$  erg s $^{-1}$  cm $^{-2}$ ) flux limit.

The left panels show models with different L–T correlation within our default model with  $(s, \sigma_\ell, \ln L_{15,0}) = (1.0, 0.59, 1.81)$ . The survey is mass-complete at 4 keV out to  $z \sim 0.7$ , independent of  $r$ , giving counts that are identical in this redshift range. The mean luminosities shift from the mass-limited mean by an amount  $r \sigma_\ell \langle \delta_t \rangle$ , where  $\langle \delta_t \rangle$  is the mean temperature deviation of the selected sample. For halos of fixed temperature, the steepness of the mass function implies that  $\langle \delta_t \rangle > 0$ ; there are more low-mass halos to scatter upward into the temperature bin than high-mass halos to scatter downward. This effect either brightens or dims the mean luminosity at low redshifts, depending on the sign of the correlation,  $r$ . At  $z \gtrsim 0.7$ , the differences in 4 keV mass selection among the models become appreciable. Compared to the  $r = 0$  case, this selection effect drives the counts up and the mean masses down for the  $r = 0.7$  model, and vice-versa for  $r = -0.7$ . The magnitude of this mass shift is small, however, amounting to  $-3\%$  and  $+6\%$  at  $z = 1.5$ , respectively.

The right panels of Fig. 4 show two zero correlation models tuned to produce behavior similar to the  $r = \pm 0.7$  cases. The parameter sets,  $(s, \sigma_\ell, \ln L_{15,0}) = (1.10, 0.35, 1.95)$  and  $(0.95, 0.72, 1.65)$ , are within the 95% error contours that result from the REFLEX analysis of Stanek et al. (2006). The solid line reproduces our default model, as in the left panels, where  $r = 0$ . The luminosity moments and sky surface densities of these models lie within a few percent of the respective covariance models shown in the left panels, but the driving mechanisms are different. The dimmer intercept and larger scatter of the  $s = 0.95$  case force this model to become mass-incomplete earlier than the default case. The counts drop beyond  $z \gtrsim 0.7$  and the mean luminosity rises as the Malmquist bias is triggered. The  $s = 1.10$  case, with a smaller scatter and higher intercept, remains mass-complete to a higher redshift, leading to larger counts and a smaller Malmquist bias.

Unlike the  $r = \pm 0.7$  case, the mean halo mass selected by the 4 keV constraint is not shifted at high redshift in these models. When  $r = 0$ , halos that scatter up or down into a fixed temperature bin are equally likely to be culled by the sample flux limit. Mass estimates from weak lensing of stacked ensembles could potentially be a useful discriminatory diagnostic, but systematic effects must be controlled at the one-percent level at  $z \approx 1$ . The upside is that next-generation surveys will produce large numbers of high- $z$  clusters. According to Fig. 4, a 5000-square degree, deep-flux limit survey will yield 445 clusters with temperatures between 3.8 and 4.2 keV, and between 0.9 and 1.1 in redshift.

#### 4 CONCLUSIONS

The multivariate properties of massive halos selected by X-ray flux-limited surveys are sensitive to assumptions about the correlation between bulk observable properties at fixed mass. Using a model in which the L–M relation is tuned to match local REFLEX counts, we show how the Malmquist bias in mean luminosity (which arises from mass-incompleteness) disappears during the transition from shallow to deep flux-limited samples. Although the underlying model is based on power-law behavior, the geometric mean L–M relation from a flux-limited sample will deviate from a pure power-law, with a kink at the mass scale above which the survey becomes mass-complete. For a survey with a flux limit,  $10^{-14}$  erg s<sup>-1</sup> cm<sup>-2</sup>, this feature is expected to lie near  $M = 2 \times 10^{14} h^{-1} M_{\odot}$ .

Using a model with Gaussian covariance to describe how  $L$  and  $T$  jointly relate to mass and redshift, we compute luminosity moments and sky counts of clusters at fixed X-ray temperature. The slope and scatter of the L–T relation for bright, local samples is sensitive to the covariance between these properties. Placing limits on the covariance from local samples will require prior information on the intrinsic  $L$  and  $T$  variance at fixed mass, and such priors can be obtained from external observations or from gas dynamic simulations.

Finally, we address attempts to extract information on cluster evolution from the behaviour of the L–T relation within a flux-limited survey. We show that non-zero L–T covariance affects counts and luminosity moments as a function of redshift in a manner that is degenerate with redshift evolution at zero covariance.

A deep X-ray survey of clusters, by itself, is limited to the information provided by counts and moments. Combining such a sample with optical and sub-millimeter observations offers the potential to break the evolution-covariance degeneracies through lensing-mass estimates and additional signatures that can be computed via extensions to the approach introduced in this paper.

We thank Kerby Shedden and Chris Mullis for valuable conversations. This work is supported by the Michigan Space Grant Consortium, by NASA grant NAG5-13378, by NSF ITR grant ACI-0121671 and by NASA through Chandra Postdoctoral Fellowship grant number PF6-70042 awarded by the Chandra X-ray Center, which is operated by the SAO for NASA under contract NAS8-03060. AEE acknowledges support from the Miller Foundation for Basic Research in Science at University of California, Berkeley. Simulations used in this paper were carried out by the Virgo Supercomputing Consortium using computers based at the Computing Centre of the Max-Planck Society in Garching and at the Edinburgh parallel Computing Centre. The data are publicly available at <http://www.mpa-garching.mpg.de/NumCos>.

#### APPENDIX A: K-CORRECTION

To convert rest frame to observed soft-band (0.5 – 2.0 keV) flux, we multiply the former by a correction factor obtained from fitting the output of an 0.3 solar metallicity `mekal` plasma model. Specifically, we use  $L_{\text{obs}} = K(z, kT) L_{\text{rest}}$

with

$$K(z, kT) = 1 + z [K_1(kT) + K_2(kT) z] \quad (\text{A1})$$

$$K_1(kT) = -0.209 + \log kT(1.18 - 0.39 \log kT)$$

$$K_2(kT) = -0.098 + \log kT(-0.092 + 0.085 \log kT),$$

and  $kT$  in keV. The fit is accurate to a few percent within  $z = 2$ .

#### REFERENCES

- Arnaud M., Evrard A. E., 1999, MNRAS, 305, 631  
 Balogh M. L., Babul A., Voit G. M., McCarthy I. G., Jones L. R., Lewis G. F., Ebeling H., 2006, MNRAS, 366, 624  
 Böhringer H., et al., 2002, ApJ, 566, 93  
 Böhringer H., et al., 2006, The Messenger, 123, 49  
 Bower R. G., 1997, MNRAS, 288, 355  
 Ebeling H., et al., 1998, MNRAS, 301, 881  
 Evrard A. E., et al., 2002, ApJ, 573, 7  
 Evrard A. E., Metzler C. A., Navarro J. F., 1996, ApJ, 469, 494  
 Fabian A. C., Cutri R. M., Smith H. E., Crawford C. S., Brandt W. N., 1996, MNRAS, 283, L95  
 Fairley B. W., et al., 2000, MNRAS, 315, 669  
 Holder G. P., Carlstrom J. E., 2001, ApJ, 558, 515  
 Kaiser N., 1986, MNRAS, 222, 323  
 Koester B. P., et al., 2007, astro-ph/0701265  
 Kotov O., Vikhlinin A., 2005, ApJ, 633, 781  
 Levine E. S., Schulz A. E., White M., 2002, ApJ, 577, 569  
 Lima M., Hu W., 2004, Physical Review D, 70, 043504  
 Lima M., Hu W., 2005, Physical Review D, 72, 043006  
 Lumb D. H., et al., 2004, A&A, 420, 853  
 Majumdar S., Mohr J. J., 2004, ApJ, 613, 41  
 Markevitch M., 1998, ApJ, 504, 27  
 Maughan B. J., Jones L. R., Ebeling H., Scharf C., 2006, MNRAS, 365, 509  
 Miller C. J., et al., 2005, AJ, 130, 968  
 Mushotzky R. F., Scharf C. A., 1997, ApJL, 482, L13  
 Novicki M. C., Sornig M., Henry J. P., 2002, AJ, 124, 2413  
 O’Hara T. B., Mohr J. J., Bialek J. J., Evrard A. E., 2006, ApJ, 639, 64  
 Pierre M., et al., 2006, MNRAS, 372, 591  
 Poole G. B., Babul A., McCarthy I. G., Fardal M. A., Bildfell C. J., Quinn T., Mahdavi A., 2007, preprint (astro-ph/0701586)  
 Reiprich T. H., 2006, A&A, 453, L39  
 Reiprich T. H., Böhringer H., 2002, ApJ, 567, 716  
 Rowley D. R., Thomas P. A., Kay S. T., 2004, MNRAS, 352, 508  
 Scharf C. A., Jones L. R., Ebeling H., Perlman E., Malkan M., Wegner G., 1997, ApJ, 477, 79  
 Spergel D. N., et al., 2006, preprint (astro-ph/0603449)  
 Stanek R., Evrard A. E., Böhringer H., Schuecker P., Nord B., 2006, ApJ, 648, 956  
 Vikhlinin A., VanSpeybroeck L., Markevitch M., Forman W. R., Grego L., 2002, ApJL, 578, L107